Tunable nanoscale localization of energy on plasmon particle arrays

René de Waele, A. Femius Koenderink, and Albert Polman*

Center for Nanophotonics, FOM Institute for Atomic and Molecular Physics AMOLF, Kruislaan 407, 1098 SJ Amsterdam, The Netherlands

This paper appeared as Nano Lett. **7**, 2004-2008 (2007) [Received April 5, 2007. Published 06/09/2007]

*Corresponding author. Tel +31 20 6081234. Fax +31 20 6684106. Email: waele@amolf.nl.

ABSTRACT. We demonstrate experimentally that plasmon resonant nanoparticle chains exhibit a nanoscale localized response to unfocused light that can be controlled by tuning the incident wavelength. Confocal microscopy shows that field concentrates on just a few nanoparticles at either the front or back side of the plasmon chains. Our experiments clearly demonstrate that plasmon chains are nanoscale receivers and concentrators of light analogous to multi-element radio wave antennas. This analogy inspires new design rules for many other photonic functionalities, like guiding and redirecting light at the nanoscale.

KEYWORDS. Plasmon polaritons. Optically resonant nanoparticles. Nano antennas. Field enhancement

With the advent of novel techniques to structure materials on the nanoscale, the study of noble metal nanostructures for nanoscale photonics has gained tremendous momentum.[1,2] The key property of metal nanostructures is that light is coupled to resonant motion of the free electron plasma in the metal, which allows metal nanostructures to enhance and confine electromagnetic fields. Such plasmonic materials are therefore promising for photonic applications in nonlinear optics[3], for the control of optical signals on subwavelength length scales[1,2,4-6], but also as biocompatible labels in microscopy[7] and as agents for locally enhanced photothermal medical therapies[8]. To achieve the goal of locally enhancing electromagnetic fields in a controlled fashion, researchers have focused on so-called plasmon antennas.[9-11] These antennas operate by the local enhancement of electric field near sharp edges of metals, and the strong field that can be generated in narrow gaps between subwavelength metal islands.

Chains of coupled resonant metal particles have been proposed by Quinten *et al*.[4] and Brongersma *et al.*[5] to allow transport of confined plasmon excitations from particle to particle at nanometer length scales. An intuitive picture is that waveguiding occurs below the diffraction limit and without radiation loss via instantaneous 'quasi-electrostatic' near-field dipole-dipole interactions.[5,12,13] Recently, however, several theoretical reports have pointed out that the dispersion relation for such guiding can be phasematched to the dispersion relation of free photons around the arrays, even for arrays with

subwavelength spacings as small as 75 nm.[14-17] Around this condition, plasmon nanoparticle chains couple particularly strongly to incident light. Moreover, since interaction between particles occurs via (retarded) far-field contributions, the local response of plasmon chains is expected to be extremely sensitive to the frequency of incident light, due to interference effects.[14,18] This effect can be used to capture light from an incident plane wave and create strongly localized tunable energy distributions as first proposed by Hernández *et al*.[14]

In this Letter we use confocal microscopy to image the local distribution of electromagnetic intensity near plasmon chains with subwavelength spacing in response to illumination along the array axis. The response is not spread out evenly over the entire array, but is located either at the front few particles, or at the backmost particles of the array. The exact distribution can be controlled via the incident wavelength.[14] Such a strong local response to far field radiation on a single site of an array is equivalent to the response of radio wave antennas, in which an array of resonant scatterers is used to optimize constructive interference for maximum signal on a single electrically connected element.[19,20]. Plasmon particle chains are equivalent to such multi-element radio wave antennas, apart from the source of the resonance of individual buildings blocks. Whereas in the case of RF antennas, the resonance derives its existence entirely from the scatterer size, in the optical case resonant scattering requires a material resonance. Our work thus demonstrates a new paradigm for nano-antenna design: instead of relying on edges or gaps to create field singularities, one can engineer the interferences in radiative coupling between many resonant antenna elements to efficiently funnel light into a nanoscale spot.

Silver nanoparticle chains were fabricated using electron-beam lithography and lift-off on fused silica substrates. Figure 1a shows a scanning electron microscopy image of three typical arrays. Each array consists of ten particles with lateral dimensions of 110 nm x 110 nm and height of 50 nm. The center-to-center distance between adjacent particles within arrays is 150 nm and the arrays are separated by 1.7 μm, at which plasmon interaction between the chains is negligible. Samples were subsequently embedded in index matching oil (n= 1.46) and sandwiched between a pair of glass cover slips. A supercontinuum white light source was used to optically excite the nanoparticle chains. A

monochromator enabled tuning of the excitation wavelength between 450 nm and 850 nm. Using an optical fiber we guided the excitation beam into the layer of index matching oil embedding the sample, and illuminated the arrays sideways along the array axis (Fig. 1b). Light that was scattered in the upward direction by the nanoparticle arrays was collected by a microscope objective (60x, NA=0.8) in an infinity-corrected confocal microscope arrangement. The collected light was focused onto a 25 μm diameter confocal pinhole using a f=160 mm tube lens, and was subsequently detected by an avalanche photodiode. Two-dimensional confocal images were acquired by simultaneously scanning sample and excitation fiber with a piezoelectrically driven scanning stage.

Figure 2 shows confocal images of the topmost array in Fig. 1a under irradiation with the excitation beam directed along the array. Incident light travels from left to right in the images. The position of the array is schematically indicated by the circles. Figure 2a shows the optical response of the array at an excitation wavelength of 600 nm. At this wavelength, most of the scattered light is recorded from the front side of the array, i.e. from the side that is first encountered by the excitation beam. The optical behaviour of the array dramatically changes when the wavelength is tuned to 700 nm (Fig. 2b). Most of the light is now scattered at the back side of the array. These images demonstrate that we can controllably concentrate light on just a few nanoparticles using unfocused illumination at a wavelength close to the single-particle resonance (λ= 650 nm).

To study the transition of the response that is shown in Fig. 2 in more detail, we plot the optical response for multiple excitation wavelengths from 550 to 800 nm in Fig. 3a. The graphs in the figure were obtained by summing the signal along the lateral direction of the recorded confocal images, i.e. perpendicular to the array axis. The curves in Fig. 3a are all normalized and plotted with an offset for clarity. The figure also depicts the location of the particle array and the propagation direction of the incident light beam. We find that for the shorter wavelengths the front side of the array is preferentially excited, while the backmost particles become preferentially excited at longer wavelengths. The transition between these two regimes occurs abruptly around λ= 675 nm within a bandwidth much

narrower than the plasmon linewidth and when the particle spacing is equal to about one third of the wavelength in the embedding medium ($d \sim \lambda/3$).

To analyse these observations we have performed calculations of the field distribution for a chain of ten coupled silver nanoparticles, similar to the model by Hernández *et al.*[14] Optical constants were derived from reference 21. The model approximates nanoparticles by point-dipoles[14-17] and yields the dipole moment ($\boldsymbol{p_n}$) induced on each particle as a function of the incident wavelength. Strictly speaking, the particles in our experiment are oblate, causing a splitting of the single-particle resonance[22,23]. This splitting can be taken into account by introducing a polarizability tensor, rather than a scalar polarizability to describe the reponse of individual particles[22]. However, the anisotropy need not be taken into account to analyze our experiment. Based on Ref. 23 we find that the blue-shifted resonance occurs at $\lambda \sim 475$ nm outside our data set, and that it is an order of magnitude weaker in absolute cross-section than the red-shifted mode. Due to dynamic depolarization, the resonance wavelength of the red-shifted mode almost coincides with that of a plasmon sphere of the same diameter (110 nm). A detailed vectorial analysis of the detection optics[24] further shows that the out-of-plane polarization corresponding to the blue-shifted mode is very inefficiently detected relative to the in-plane polarization corresponding to the red-shifted mode (contrast 1:50). The blue-shifted mode can hence be ignored, and we use the scalar polarizability of a silver nanosphere of the same radius as the oblate semimajor axis.

It is important to realize that phase retardation as well as radiative and non-radiative loss mechanisms are fully taken into account in our point-dipole description. Indeed, phase retardation and interference are crucial for the phenomena in Figures 2 and 3: if we only include near-field interactions as in the commonly used quasistatic model,[3,5,12,13] we do not observe any asymmetric energy distribution on the array. The calculations were done for plane wave excitation and a refractive index of the surrounding dielectric medium of 1.46. We find a strong localization of the power ($\propto |\boldsymbol{p_n}|^2$) on the frontmost sphere for excitation at short wavelengths. In agreement with the experimental results we find that the backmost particle of the array becomes preferentially excited for wavelengths longer than approximately 675 nm. The colored spheres in the bottom and top part of Fig. 3b show how the dipole moments are

distributed over the particles in the chain for the short (λ= 550 nm) and long (λ= 800 nm) wavelength case respectively. These calculations show that the power is truly confined to only one or two spheres in the chain at a position that can be tuned through the incident wavelength.

To directly compare the dipole model with the experimental observations we need to account for the microscope collection optics, keeping in mind that radiation from many coherently coupled dipoles within the focus interferes at the confocal pinhole. Therefore we use a vectorial amplitude point spread function[24] to translate the calculated dipole moments into far field intensity profiles (Fig. 3b), that can be compared to the experimental data in Fig. 3a. We see excellent qualitative agreement between the experimental and calculated data, especially regarding the frequency range of the transition.

For a quantitative comparison we consider the response from the front and back side of the array for wavelengths around the observed transition wavelength (Fig. 4). The curves in Fig. 4a are for the experiment and intersect at a wavelength of about 650 nm, while the calculated curves in Fig. 4b show a crossover wavelength of approximately 660 nm, very close to the experiment. For wavelengths far away from the intersection point (λ< 550 nm, λ> 775 nm) the energy in the chain becomes more delocalized, which causes a reduced contrast between front and back side of the array. Both calculated curves in Fig. 4b show oscillations in the intensity contrast for excitation wavelengths close to or longer than the crossover wavelength. These variations are not observed in the experimental curves. We attribute this to particle size and position disorder in the array. The silver nanoparticles used in the experiment have a 5% spread in diameter as observed with scanning electron microscopy. Monte Carlo simulations including this level of disorder yield an ensemble averaged crossover wavelength of 668 ± 15 nm. Our calculations also show that the intensity contrast between the front and back side of the array depends on the disorder. For applications the required fabrication accuracy will ultimately depend on the desired functionality.

To understand the response of plasmon particle chains we note a one-to-one correspondence with radio antenna arrays first proposed by Yagi and Uda.[19,20] Such antenna receivers consist of a single dipole that is electrically connected to read out the radio signal, and that is embedded in an array of

regularly spaced scatterers that have a resonant response around the operating frequency. The role of the dipole scatterers is to enhance the signal by optimizing the constructive interference of the incident field and scattered fields at the read-out dipole. For Yagi-Uda antennas signal reception is optimal on the backmost end of the antenna when the spacing is around ~ $\lambda/3$ and when the array points into the source direction, as in our experiment (Fig. 2b). Since dipole-array antennas rely on the combination of a dipole resonance and optimized geometry for interference, their response is strongly directional and sharply frequency-dependent as in Figure 4. The description of plasmon chains as coupled point-dipole arrays is equivalent to that of dipole array radio antennas, yet downsized to nanometer scale and operating at optical frequencies. There is one important conceptual difference however:[13] while radio engineers need to create a geometrical resonance in the single building-block shape, the single building-block resonance in plasmon arrays requires a resonant material response. Control over the exact resonance frequency, linewidth and polarization anisotropy of single building blocks can be obtained both by changing the material response (i.e., using different metals) and by varying the particle geometry to be, e.g., ellipsoidal or layered in a core-shell geometry, rather than spherical.[8,22]. Plasmon materials are unique in providing the requisite material resonance for subwavelength nanoparticles: indeed our model shows that no tunable energy localization occurs for dielectric dots of similar size. Intuitively one might expect that Ohmic damping is the main drawback of using a material resonance. However, a Mie calculation shows that for our silver particles the albedo is almost 0.95, implying that 95% of the damping of a single particle resonance is radiative, and only 5% is absorptive. Indeed, removing Ohmic damping from our model does not affect either the plasmon resonance linewidth or the energy localization.

In conclusion, we have shown that the resonant optical response in a metal nanoparticle chain, illuminated with unfocused light, can localize on just a few particles at either the front or back side of the array. By tuning the wavelength of the incident light we can actively control which side of the array becomes excited. Optimizing field enhancements locally by using arrays of many resonant antenna elements as in this work is complementary to, and can be advantageously combined with current approaches to optical antennas that rely on shape singularities.[9-11] Finally, we point out that our work

invalidates a common design approach in plasmonics: it is the first experiment to invalidate the commonly accepted quasistatic approximation that coupling to far-field radiation is unimportant for subwavelength nanoparticle configurations, since energy localization is not observed in the quasistatic model. As a consequence many existing proposals to use subwavelength plasmon particle arrays need to be critically reassessed. For instance, our experiment implies that guiding of light below the diffraction is not limited by Ohmic damping,[5,12] but by radiative loss.[15-17] While coupling to radiation can be suppressed for guiding,[17] enhancing it also offers exciting new opportunities based on the antenna phenomena demonstrated in our work: this includes many applications in nanoscale optoelectronics, nonlinear optics, sensing, ultrasmall directional light sources and wavelength tuneable nanolithography.[18]

Acknowledgement. We thank L. Kuipers and L. D. Noordam for stimulating discussions. This work is part of the research program of the "Stichting voor Fundamenteel Onderzoek der Materie (FOM)," which is financially supported by the "Nederlandse Organisatie voor Wetenschappelijk Onderzoek (NWO)." It was also supported by "NanoNed", a nanotechnology program funded by the Dutch Ministry of Economic Affairs.

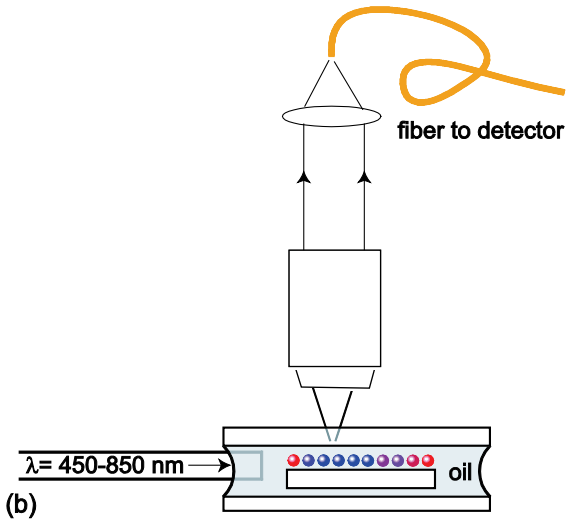

Figure 1. Scanning electron microscopy image of silver nanoparticle arrays and schematic overview of the experimental setup. (a) Finite arrays of silver nanoparticles with dimensions 110 nm × 110 nm × 50 nm (height) on a substrate of silica, imaged by scanning electron microscopy. (b) Schematic drawing of the experimental setup. The substrate with the nanoparticles is embedded in index matching oil (n=1.46). An optical fiber (core diameter 100 μm) is used to direct the light (bandwidth 5 nm) into the oil layer along the particle chains. The localized optical response of the arrays is probed in a confocal microscope with 60× objective (numerical aperture 0.8).

Figure 2. Two-dimensional confocal images of an array with ten silver particles (coloured circles) that is illuminated from the left along the array axis. (a) For excitation of 600 nm the response localizes on the front part of the array. (b) At 700 nm the back side of array is preferentially excited. Pixel integration time for both images was 50 ms.

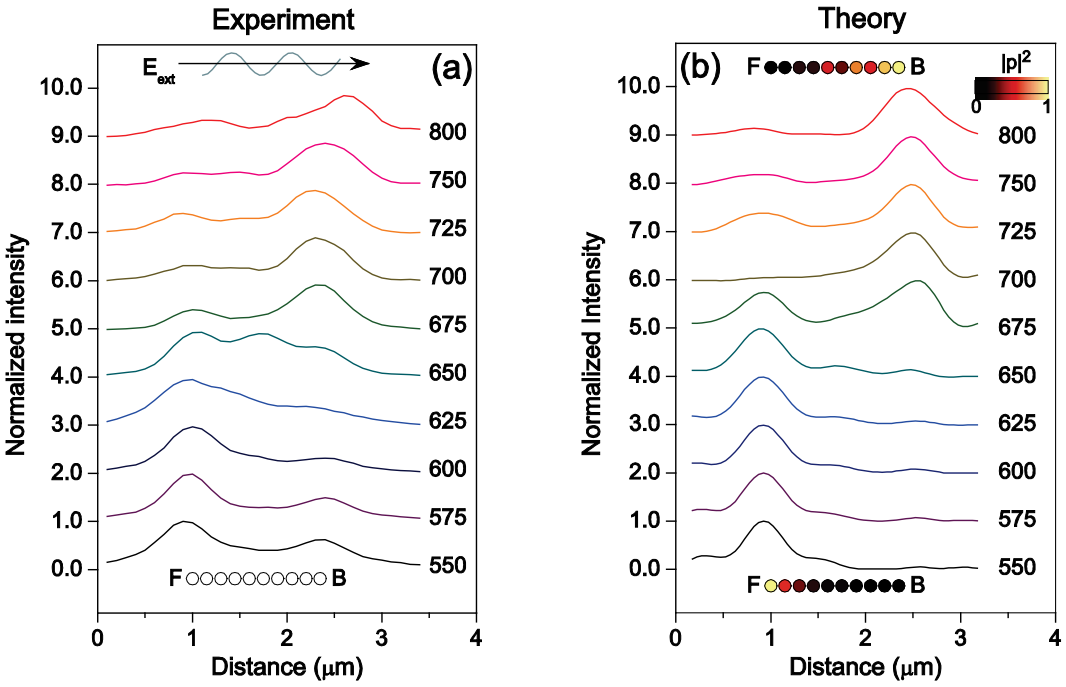

Figure 3. Comparison between the measured and calculated optical response of a silver nanoparticle array. (a) Optical response measured for wavelengths from 550 to 800 nm. The curves were obtained by summing intensity maps as in Fig. 2 along the lateral dimension, i.e. perpendicular to the array axis. Light travelled from left to right in the image and the position of the array is indicated by the open circles. The localized response is strongest on the front (F) side of the array for wavelengths below 675 nm and strongest on the back (B) side for longer wavelengths. (b) Calculated optical response of the array, obtained using a dipole coupling model, taking into account retardation and (non-)radiative loss, show similar behaviour. The coloured circles at the bottom and top of panel (b) show the relative ohmic power on each sphere of the array, for excitation at 550 and 800 nm respectively. In the short wavelength case the energy is confined to the leftmost sphere, while for the longer wavelength the energy localizes on the rightmost spheres.

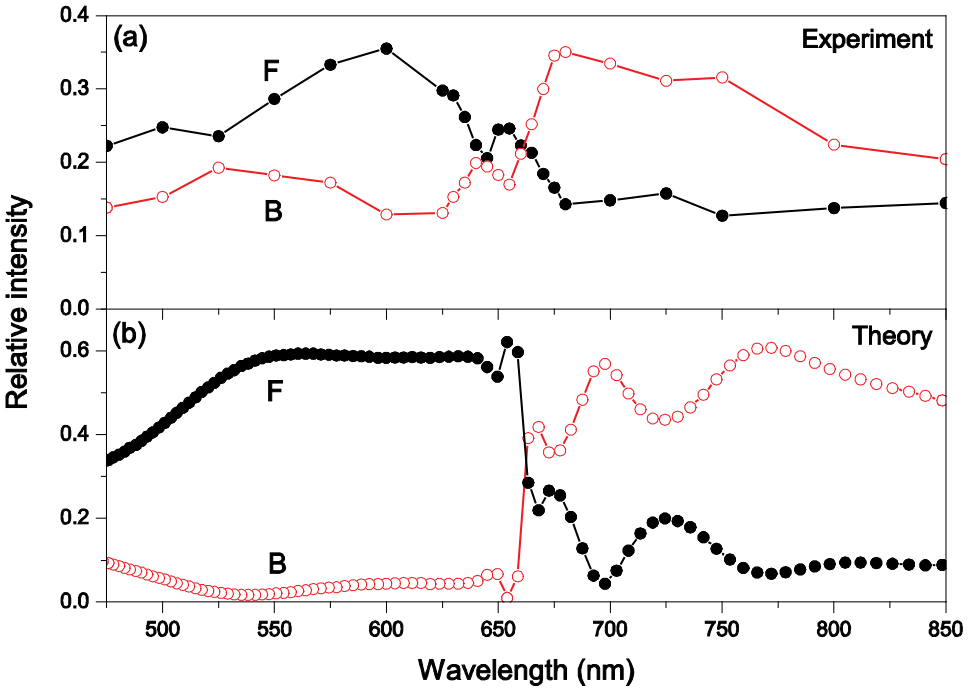

Figure 4. Ratio between the optical response from front and back side of the array as a function of wavelength. (a) Relative contribution to the total signal recorded from the front (F, closed circles) and back (B, open circles) of the array. The localized response is obtained by summing of the signal over an area of 500 nm (parallel) × 1000 nm (lateral) around the front- or backmost sphere of the array, normalized by the integrated signal over the whole array. (b) Calculated relative contributions to the far field intensity by front and back side of the array.

References.

(1) Barnes, W. L.; Dereux, A; Ebbesen, T. W. *Nature* **2003**, *424*, 824-830.

(2) Ozbay, E. *Science* **2006,** *311*, 189-193.

(3) Genov, D. A.; Sarychev, A. K.; Shalaev, V. M.; Wei, A. *Nano Lett.* **2004** *4*, 153-158.

(4) Quinten, M.; Leitner, A.; Krenn, J. R.; Aussenegg, F. R. *Opt. Lett.* **1998** *23*, 1331-1333.

(5) Brongersma, M. L.; Hartman, J. W.; Atwater, H. A. *Phys. Rev. B* **2000** *62*, R16356-R16359.

(6) Krenn, J. R.; Dereux, A.; Weeber, J. C.; Bourillot, E.; Lacroute, Y.; Goudonnetet, J. P.; Schider, G.; Gotschy, W.; Leitner, A.; Aussenegg, F. R.; Girard C. *Phys. Rev. Lett.* **1999** *82*, 2590-2593.

(7) Jacobsen, V.; Stoller, P.; Brunner, C.; Vogel, V.; Sandoghdar, V. *Opt. Lett.* **2006**, *14*, 405-414.

(8) Loo, C.; Lowery, A.; Halas, N. J.; West, J. L.; Drezek, R. *Nano Lett.* **2005**, *5*, 709-711.

(9) Schuck, P.J.; Fromm, D.P.; Sundaramurthy, A.; Kino, G.S.; Moerner, W.E. *Phys. Rev. Lett.* **2005** *94*, 017402.

(10) Mühlschlegel, P.; Eisler, H.-J.; Martin, O.J.F.; Hecht, B.; Pohl, D.W. *Science* **2005** *308*, 1607-1609.

(11) Cubukcu, E.; Kort, E.A.; Crozier, K.B.; Capasso, F. *Appl. Phys. Lett.* **2006** *89*, 093120.

(12) Maier, S.A.; Kik, P.G.; Atwater, H.A.; Meltzer, S.; Harel, E; Koel, B.E.; Requicha, A.A.G. *Nature Mater.* **2003** *2*, 229-232.

(13) Engheta, N.; Salandrino, A.; Alù, A. *Phys. Rev. Lett.* **2005** *95*, 095504.

(14) Hernández, J. V.; Noordam, L. D.; Robicheaux, F. *J. Phys. Chem. B* **2005** *109*, 15808-15811.

(15) Citrin, D.S. *Nano Lett.* **2004** *4*, 1561-1565.

(16) Weber, W.H.; Ford, G.W. *Phys. Rev. B* **2004** *40*, 125429.

(17) Koenderink, A.F.; Polman, A. *Phys. Rev. B* **2006** *74*, 033402.

(18) Koenderink, A.F.; Hernández, J.V.; Robicheaux, F.; Noordam, L.D.; Polman, A. *Nano Lett.* **2007**, *7*, 745-749.

(19) Uda S. *J. IEE (Japan)* **1926**, 273-282.

(20) Yagi, H. *Proc. IRE* **1928** *16*, 715-741.

(21) Palik, E.D. ed., *Handbook of Optical Constants of Solids*, Adacemic: Orlando, FL, 1985.

(22) Bohren, C. F.; Huffman, D. R. *Absorption and Scattering of Light by Small Particles*, Wiley, New York, 1983.

(23) Kelly, K. L.; Coronado, E.; Zhao, L. L.; Schatz, G. C., *J. Phys. Chem. B* **2003** *107*, 668-677.

(24) Haeberlé, O.; Ammar, M.; Furukawa, H.; Tenjimbayashi, K.; Török, P. *Opt. Express* **2003** *11*, 2964-2969.

Proposed graphics for table of contents.